Vol. 599: 75–91, 2018
https://doi.org/10.3354/meps12627

MARINE ECOLOGY PROGRESS SERIES
Mar Ecol Prog Ser

Published July 12

Oxygen metabolism of intertidal oyster reefs measured by aquatic eddy covariance

Martin P. Volaric*, Peter Berg, Matthew A. Reidenbach

Department of Environmental Sciences, University of Virginia, Charlottesville, Virginia 22904, USA

ABSTRACT: Oyster reef restoration is pursued at numerous places worldwide, yet little is known about how ecosystem function changes as these reefs develop. In this study, we used the non-invasive aquatic eddy covariance technique to measure the *in situ* oxygen flux of 4 intertidal sites on the Virginia (USA) coast: a natural oyster reef, 2 restoration reefs, and a mudflat. Oyster densities of the 3 reefs were 350, 295, and 186 oysters m^{-2}. Mean summer values of nighttime oxygen flux ($Flux_{DARK}$) were −488, −428, −300, and −56 mmol m^{-2} d^{-1} over the natural reef, 2 restoration reefs, and mudflat, respectively. All 4 sites had smaller daytime vs. nighttime oxygen uptake, with mean summer differences between $Flux_{DARK}$ and $Flux_{LIGHT}$ of 360, 250, 239, and 27 mmol m^{-2} d^{-1}. Light was an important short-term driver of daytime reef oxygen flux due to its effect on microalgal photosynthesis. All 3 oyster reefs were significantly heterotrophic, with summer net ecosystem metabolism values ranging from −157 to −298 mmol m^{-2} d^{-1}. $Flux_{DARK}$ values were similar across the 3 reefs when normalized by density, with values between −1.8 and −2.3 mmol m^{-2} d^{-1} $oyster^{-1}$. This study represents the most detailed measurements to date of *in situ* oyster reef oxygen flux, and shows that benthic microalgae can significantly impact reef oxygen dynamics. $Flux_{DARK}$ values scale with oyster density, and consequently can be used as a metric for reef restoration success.

KEY WORDS: *Crassostrea virginica* · Oxygen flux · Net ecosystem metabolism · Production · Hydrodynamics · Benthic microalgae

INTRODUCTION

Oysters are key ecosystem engineers that inhabit many coastal waters and form high-relief, 3-dimensional reef systems. These reefs act as habitat for a variety of benthic infauna, forming complex reef communities. Oyster reefs perform a wide range of ecosystem services, including filtering organic and inorganic particulate matter from the water column (Newell 1988, Nelson et al. 2004), mitigating the negative effects of plankton blooms/die-offs, and preventing erosion of salt marshes (Coen et al. 2007). In performing all of these services, oyster reefs improve overall water quality (Coen et al. 2007).

Global oyster populations have been significantly depleted, as oyster reef habitat has declined worldwide by approximately 85% over the past 130 yr (Lotze et al. 2006, Beck et al. 2011). This decline has affected multiple oyster species (Kirby 2004) and is due primarily to overharvesting (Jackson et al. 2001). Populations of the eastern oyster *Crassostrea virginica*, which form reefs along the US eastern and gulf coasts, have additionally been devastated by the diseases MSX (*Haplosporidium nelson*) and Dermo (*Perkinsus marinus*) (Rothschild et al. 1994, Oliver et al. 1998), resulting in a decline in reef extent of 90–99% across this region (Kemp et al. 2005, Beck et al. 2011).

In order to combat this decline, many efforts have been made to restore oyster reefs, and there have been successful restorations in both North America and Europe (Beck et al. 2011). Along Virginia's East-

*Corresponding author: mpv3a@virginia.edu

ern Shore, The Nature Conservancy (TNC), in partnership with state and federal agencies, has been conducting large-scale efforts to restore *C. virginica* reefs. TNC has attempted a wide variety of strategies to restore oyster reefs, including the use of piled *C. virginica* shell, piled *Busycotypus canaliculatus* whelk shell, and oyster castles. The goal of these efforts is to create hard elevated structural habitat that serves as suitable settlement sites for oyster larvae (Whitman & Reidenbach 2012). The vertical extent of these oyster reefs is of great importance, as it helps prevent sedimentation of the reef (Schulte et al. 2009) and provides suitable water column flow and turbulence conditions that can attract and retain pelagic oyster larvae (Fuchs & Reidenbach 2013, Hubbard & Reidenbach 2015, Fuchs et al. 2015).

Oyster reefs are diverse communities that contain numerous benthic infauna such as xanthid crabs, polychaete worms, and amphipods (Rodney & Paynter 2006), as well as various micro- and macroalgae (Thomsen & McGlathery 2006). Given the complex nature of these ecosystems, it can be difficult to derive parameters that describe the entire reef community. Oxygen flux represents one such attribute, as it can be used as a proxy for the integrated carbon metabolism of the system (Glud 2008). Measurements of oxygen flux give insight into the health and function of oyster reefs, and allow for the identification of environmental drivers that stimulate reef functioning. They also inform how oyster reefs alter water column chemistry. For example, oxygen uptake by oyster reefs is positively correlated to denitrification (Kellogg et al. 2013, Humphries et al. 2016, Smyth et al. 2016).

Past studies of oxygen flux over oyster reefs have shown that these are strongly heterotrophic systems that have a large oxygen demand, with uptake values as high as 3000 mmol m^{-2} d^{-1} (Dame et al. 1992) and 932 mmol m^{-2} d^{-1} (Kellogg et al. 2013). However, these experiments either used flow chambers, which isolate the oysters from the surrounding environment to create a distinct control volume, or chamber incubations conducted *ex situ* in a laboratory setting. As a result, previous studies to quantify changes in dissolved oxygen levels have interfered with the flow environment and light conditions, and have been unable to identify key drivers of oyster reef oxygen flux under natural conditions. Eddy covariance has long been the preferred methodology for quantifying scalar fluxes in the atmosphere (e.g. Priestley & Swinbank 1947), and has more recently been adapted for measuring benthic oxygen fluxes (Berg et al. 2003). This technique has several advantages over other flux methods, including its non-invasive nature (Lorrai et al. 2010), ability to integrate over a large benthic surface (Berg et al. 2007), and high temporal resolution (Rheuban & Berg 2013). These advantages allow for the quantification of oxygen uptake values of the reef community in combination with simultaneous measurements of environmental parameters such as flow speed and light, enabling the identification of key environmental drivers of oyster reef oxygen fluxes which cannot be accomplished via other techniques. Aquatic eddy covariance has been successfully used to quantify oxygen fluxes and their controls under natural conditions over a large variety of complex benthic ecosystems, including hard bottom substrates (Glud et al. 2010), seagrass meadows (Hume et al. 2011, Rheuban et al. 2014a,b, Long et al. 2015), coral reefs (Long et al. 2013, Rovelli et al. 2015), and coralline algal beds (Attard et al. 2015).

As young restoration reefs grow, there should be an increase in benthic oxygen demand that scales with the total biomass of the reef community. Additionally, as reefs accrete new individuals, an increase in 3-dimensional structure allows for a greater surface area for benthic micro- and macroalgae to attach, so reefs of different size and complexity may have different quantities of primary producers which release oxygen. To date, only one previous study of oxygen flux over an oyster reef using aquatic eddy covariance has been conducted, but this was a proof-of-concept study confined to a single reef during 1 wk in the summer (Reidenbach et al. 2013). Our study built upon these findings by comparing seasonal flux measurements and integrated benthic metabolism over a natural oyster reef, 2 restoration oyster reefs of different age and oyster density, and an adjacent intertidal mudflat. The goals of this study were to use aquatic eddy covariance measurements to (1) describe how oyster reef metabolism changes as reefs mature, (2) identify the environmental controls of oyster reef oxygen flux, and (3) quantify the relative success of 2 oyster reef restorations.

MATERIALS AND METHODS

Study sites

The study sites were located within the Hillcrest Oyster Sanctuary, a network of intertidal oyster reefs monitored by TNC in the shallow coastal bays of Virginia's Eastern Shore (Fig. 1). This sanctuary is within the Virginia Coast Reserve (VCR), part of the National Science Foundation's Long Term Ecological

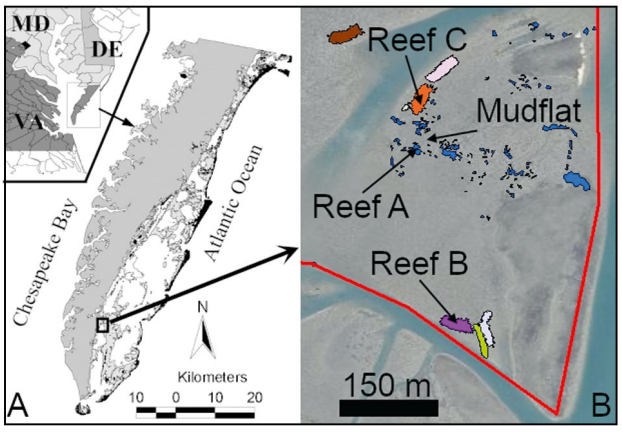

Fig. 1. (A) Location of Hillcrest Oyster Sanctuary off the coast of the Delmarva Peninsula, Virginia, USA. (B) Different colors denote different reefs restored by The Nature Conservancy (TNC), with blue representing natural reefs that existed prior to any restoration efforts. The red line shows the boundary of the sanctuary (image provided by TNC)

Research (LTER) network. Four sites were chosen for comparative analyses: 3 oyster reefs of various age and density, and 1 intertidal mudflat (Fig. 2). Reef A is one of several oyster reefs at the VCR that were originally established by local watermen in the 1950s and 1960s but have not been actively managed since. Having existed prior to any restoration efforts by TNC, it is considered by TNC to be a natural oyster reef. It measures 240 m^2 in size (22.5 m long × 10.5 m wide), and has a mean ± SE oyster density of 350 ± 62 oysters m^{-2} (n = 4). Reef B is a restoration oyster reef established by TNC in 2010 using piled oyster shell. It was identified by TNC as being their most successful restoration in the sanctuary reef network, which is why it was chosen for this study. Reef B measures 430 m^2 in size (27 m long × 16 m wide). It had a slightly lower but not significantly different oyster density than Reef A, with a mean density of 295 ± 35 oysters m^{-2} (n = 4). Reef C was established in

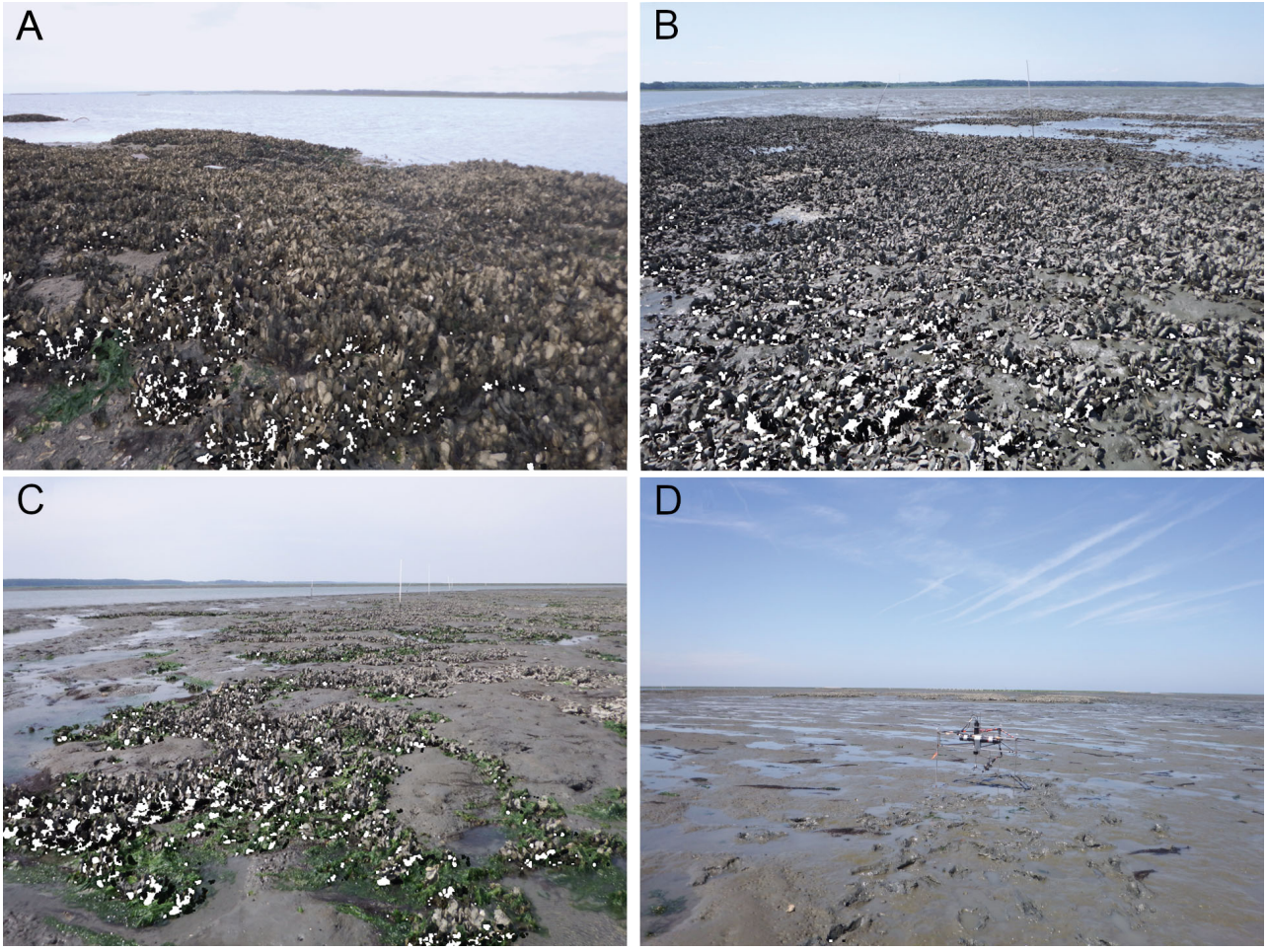

Fig. 2. Four sites were chosen for the study: (A) a natural oyster reef, (B,C) 2 reefs restored by The Nature Conservancy (TNC), and (D) an intertidal mudflat. Reef A existed prior to any restoration efforts by TNC at Hillcrest, and had a density of 350 ± 62 oysters m^{-2} (mean ± SE, n = 4 samples). Reef B was established by TNC in 2010 using piled oyster shell, and had a mean density of 295 ± 35 oysters m^{-2} (n = 4). Reef C was established by TNC in 2008 using piled oyster shell, and had a mean density of 186 ± 66 oysters m^{2} (n = 7)

2008 by TNC also using piled oyster shell. It measures 3450 m^2 in size (77.5 m long × 44.5 m wide), and has a density of 186 ± 66 oysters m^{-2} (n = 7). All density counts were made for individuals >70 mm in length using 0.25 m × 0.25 m quadrats placed randomly on the reef. Reef A also had a ribbed mussel *Geukensia demissa* density of 65 ± 14 mussels m^{-2} (n = 4), while there were no mussels present on Reef B or Reef C. The mudflat consists of an area of bare sediments on the same tidal flat as the oyster reefs, and is located approximately 75 m east of Reef A (Fig. 1B). There were no oysters or mussels on the mudflat.

Sediment organic matter content was measured (loss on ignition; 6 h at 500°C) as 3.09 ± 0.14 % (mean ± SE, n = 9) on Reef A, 3.82 ± 0.14 % (n = 9) on Reef B, 2.2 ± 0.12 % (n = 9) on Reef C, and 1.45 ± 0.07 % on the mudflat (n = 9). The tidal range at all sites is approximately 1.5 m.

Equipment and observational setup

The eddy covariance system consists of a Nortek AS Vector© acoustic Doppler velocimeter (ADV) connected to a fast-response (90 % response time ≤0.4 s) Unisense AS Clark-type oxygen microelectrode (stirring sensitivity <1 % according to the manufacturer) via a high-resolution custom-made picoamp amplifier (Berg & Huettel 2008). The ADV makes 3-dimensional high-frequency velocity measurements within a cylindrical measurement volume that is 14 mm in diameter and 14 mm in height. A specialized alignment tool attached to the ADV prior to deployment was used to locate this measurement volume, and the electrode was placed 0.5 cm from its edge so as not to interfere with ADV data collection. These instruments were then mounted on a stainless steel frame designed to minimize hydrodynamic interference (Fig. 3A), and together measured the velocity and oxygen concentration (Fig. 3B) at either 32 or 64 Hz over 15 min bursts for each deployment. Each burst consisted of a 14.5 min interval of data collection followed by a 30 s pause. The ADV and amplifier were powered by the same external battery, and the ADV's internal recorder was capable of storing up to ~60 h of 32 Hz data logging both velocity and oxygen data. The measuring height was set using a ruler during low tide reef exposure to ~10 cm from the benthos (as defined by the tops of oyster shells) for all sites. This distance was chosen to balance the smoothing of heterogeneity effects (Rheuban & Berg 2013) against the need to minimize the oxygen storage capacity of the water between the reefs and the measurement volume (e.g. Rheuban et al. 2014a).

Fig. 3. (A) Eddy covariance system deployed over Reef A at low tide. (B) The eddy covariance system consists of an acoustic Doppler velocimeter (ADV) connected to an oxygen microelectrode, and samples velocity and oxygen within the same volume of water at either 32 or 64 Hz

PME miniDOT© oxygen optodes were placed close to the eddy systems in order to calibrate the raw electrical signal measured by the microelectrodes. Photosynthetically active radiation (PAR) measurements were made using Odyssey PAR loggers, and calibrated as described by Long et al. (2012). Small wave activity was seen throughout the majority of data collection, as identified by sinusoidal patterns in the ADV velocity data. Significant wave height, defined as the average height of the highest one-third of waves, was calculated as $4\sigma_p$, where σ_p is the standard deviation of the pressure using data collected by the ADV (Wiberg & Sherwood 2008). Using this methodology, the mean significant wave height at all sites for all deployments was <0.06 m. Likewise, 99 % of the sampling interval had significant wave height <0.1 m.

A total of 4 primary data collection campaigns were performed. Two eddy covariance systems were used for each campaign, with one placed at the center of Reef A and the other positioned at the center of either Reef B, Reef C, or the mudflat. The 2 sites were then sampled concurrently in order to account for environmental fluctuations. The sampling dates were as follows: 17–24 June 2015 (Reef A and mudflat), 1–7 August 2015 (Reef A and Reef B), 23–30 September 2015 (Reef A and Reef B), and 21 June to 8 July 2016 (Reef A and Reef C). Data were only used when the Vector and oxygen microelectrode were both submerged, which given the elevation of the sites occurred approximately 4–6 h per tidal cycle or 8–12 h d^{-1}. These data records additionally contained some gaps due to sensor breakage or malfunction. In total, nearly 300 h of high-quality eddy covariance data were collected and used for further analysis.

Eddy covariance and data analysis

Following data extraction from the ADV, the 32 or 64 Hz data were averaged down to 8 Hz in order to reduce unbiased noise (Berg et al. 2009). Total oxygen flux between the oyster reef and the water column (J_{O_2}) was calculated as:

$$\overline{J_{O_2}} = \overline{w'C'} \quad (1)$$

where the overbars indicate time averaging, and w' and C' represent the instantaneous fluctuations away from the mean of the vertical velocity and oxygen concentration, respectively (Berg et al. 2003). This calculation was made using the software package EddyFluxVer3.00 (P. Berg unpubl.). For nearly all bursts (~95%), the velocity and oxygen concentration means were determined using a least-squares linear fit of the 8 Hz data over each 15 min burst (Lee et al. 2004, Berg et al. 2009). Previous statistical examinations have found that this 15 min length of time balances the inclusion of large-scale turbulent fluctuations with changes in oxygen concentration and velocity caused by tidal flow (Berg et al. 2003). Each burst was then examined for sensor malfunction due to interference with debris in the water, which is typically identified by data spikes, excessive signal noise, or variation from the optode oxygen signal (Lorrai et al. 2010, Berg et al. 2013). All data that showed signs of these anomalies were removed. Due to the presence of small waves throughout most of our data collection, no time-shift was applied to the oxygen data when calculating the flux. The bias that results from time-shifting these data in wavy conditions can be greater in magnitude and/or in the opposite direction of the true flux (Berg et al. 2015). Additionally, the presence of waves can result in 'stirring sensitive' effects on microelectrodes (Holtappels et al. 2015; described below), which can exacerbate the errors associated with a time-shift under these conditions (Reimers et al. 2016).

A small fraction of the bursts (<5%) showed signs of large-scale fluctuations in oxygen concentration, presumably due to horizontal advection of water masses of different concentrations, that were not attributable to turbulent eddies or tidal flow. In these cases, the velocity and oxygen concentration means were defined using a running average (Lee et al. 2004, Lorrai et al. 2010). In order to determine the time interval necessary to calculate an appropriate running average, we chose a 6 h representative selection of data and compared the mean flux given by a range of running average intervals to the mean flux calculated using linear detrending. The shortest averaging interval in which the running average was within 2% of the linear average was 90 s, which we chose as the running average interval (Fig. 4).

Following data quality control, 15 min intervals of data for each deployment were separated into daytime and nighttime bursts based on PAR, and all further analysis was conducted using these data. Nighttime bursts were defined as 15 min intervals in which PAR was ≤1% of maximum PAR for each campaign, while daytime bursts were defined as the remaining data. $Flux_{DARK}$ and $Flux_{LIGHT}$ were defined as the mean of all nighttime and daytime oxygen fluxes for each deployment, respectively. Due to the interplay between the diurnal and tidal cycles, data could not be collected throughout all times of the day for each deployment. Rather, high tide (and thus data collection) times were centered around midnight and noon during June 2015, August 2015, and June/July 2016 deployments, and in the morning and evening during September 2015. High tide periods around mid-

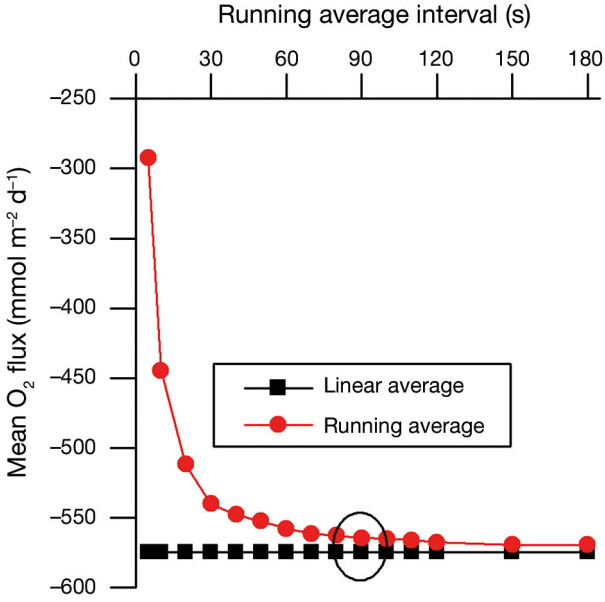

Fig. 4. Effect of averaging window on oxygen flux calculated using a running average. Most 15 min fluxes in this study were measured using means calculated via a least-squares fit to the data over a 15 min interval (linear average). However, in some cases oxygen fluctuations not due to turbulence can occur within a 15 min interval, so detrending over a shorter averaging interval (running average) should be used. Mean fluxes calculated using a running average are less than mean fluxes calculated using a linear average, but will approach the linear average at longer averaging intervals. In this case 90 s (encircled data points) was chosen as a suitable time period to calculate the running average, as it was the shortest interval in which the mean flux was within 2% of the mean flux calculated using linear averaging

night and noon were the preferred tidal cycles for measurements, as it allowed us to quantify peak $Flux_{DARK}$ and $Flux_{LIGHT}$ values.

Typically when using aquatic eddy covariance measurements covering a 24 h period, daily gross primary production (GPP) is defined as the total oxygen released over a full day (Hume et al. 2011). However, due to the intertidal nature of our measurements, combined with several possible confounding factors (described in detail in the Discussion), there is no straightforward way to calculate GPP for our sites. We instead simply calculated the difference between $Flux_{DARK}$ and $Flux_{LIGHT}$ values. Likewise, net ecosystem metabolism (NEM) is typically defined as the mean oxygen flux over a 24 h period (Hume et al. 2011). Because our sites were intertidal and did not have continuous 24 h data collection periods, we instead defined NEM as the weighted average between $Flux_{LIGHT}$ and $Flux_{DARK}$ values based on the mean length of light and dark intervals for each deployment.

Clark-type microelectrodes have been shown to exhibit 'stirring sensitivity,' whereby the instantaneous water velocity at the tip of the electrode may affect the amount of oxygen consumed by the sensor, and thus, its reading (Holtappels et al. 2015). We analyzed the potential impact of this effect on a representative nighttime dataset taken over Reef A, assuming the stirring sensitivity of the microelectrode could be described by the fitting function and parameter values (S_{sen} = 0.7 %, n = 0.65, and B = 30) presented by Holtappels et al. (2015). These specific parameters describe a case in which the electrode is pointing directly into the mean current, which is the orientation that results in maximum stirring sensitivity (Holtappels et al. 2015). We applied this function to correct our oxygen data given concurrent values of horizontal velocity and recalculated the fluxes. Overall, the difference between corrected and uncorrected fluxes was <4 %; therefore, we assert that stirring sensitivity was negligible in our data.

Hydrodynamics

For each of the 4 sites, we calculated the friction velocity ($u_\star$) from the Reynolds stress using the equation (Dade et al. 2001, Berg et al. 2007):

$$u_\star = \left(\overline{u'w'}^2 + \overline{v'w'}^2\right)^{1/4} \quad (2)$$

where u', v', and w' are the fluctuating components of horizontal, transverse, and vertical velocity, respectively, and can be calculated using the ADV data from eddy covariance measurements. In order to remove data with poorly defined inertial sublayers, bursts with velocity <2 cm s^{-1} were not included in this or any subsequent calculations involving $u_\star$. Velocity profiles over different oyster reefs on this same tidal flat have been shown to exhibit a classic logarithmic profile (Whitman & Reidenbach 2012, Reidenbach et al. 2013), so a log profile was assumed for these sites. Following the determination of $u_\star$ we calculated the sediment surface roughness parameter (z_0) as (Schlichting & Gersten 2000, Berg et al. 2007):

$$z_0 = \frac{h}{\exp\left(\frac{\overline{u_x}\kappa}{u_\star}\right)} \quad (3)$$

where h is the measuring height, κ is von Karman's constant equal to 0.41, and $\overline{u_x}$ is the mean horizontal flow velocity at the measuring height. After determining both $u_\star$ and $\overline{u_x}$, we were able to calculate the drag coefficient (C_D) using the equation (Schlichting & Gersten 2000):

$$C_D = \frac{u_\star^2}{\overline{u_x}^2} \quad (4)$$

Eddy flux measurements spatially integrate over a measurement 'footprint,' defined as the smallest benthic surface area that contributes 90 % of the flux recorded by the eddy system (Berg et al. 2007). The footprint is approximately elliptical in shape, is located directly upstream of the eddy system, and is dependent on the measuring height, water depth, and z_0 (Berg et al. 2007). For each site, we calculated both the size of the footprint, as well as the upstream horizontal distance to the location of the maximum flux contribution, as described by Berg et al. (2007).

RESULTS

Oxygen demand

Mean water-column oxygen concentrations (±SE) at the sites ranged from 180 ± 1.0 to 214 ± 0.5 µmol l^{-1} (n = 192 and 136), and tended to increase with water velocity. Current velocity magnitude (flow speed) ranged from 0 to 33 cm s^{-1} over the mudflat, 0 to 26 cm s^{-1} over Reef A, 0 to 29 cm s^{-1} Reef B, and 0 to 22 cm s^{-1} over Reef C. Data over one tidal cycle, including water velocity, oxygen concentration, oxygen flux, PAR, and water depth, are shown in Fig. 5. It is a representative example of the data that were col-

lected at all 4 sites, and shows how measurements of flux were correlated to different environmental parameters. For all oxygen fluxes, a negative flux indicates an uptake of oxygen, while a positive flux indicates a release. In this example, oxygen flux was much smaller during day than night and was occasionally positive during the hours of 13:00–14:30 h, as daylight (Fig. 5E) likely stimulated microalgal primary production. As PAR decreased, both due to an increase in water depth (Fig. 5E) and the diminishing daylight, algal photosynthesis declined and there was substantial oxygen flux towards the benthos.

Mean oxygen flux, flow speed, PAR, and temperature for both night and day at each site are shown in Fig. 6. All of the means, with the exception of temperature, represent the average of all 15 min bursts for each campaign. $Flux_{DARK}$ (±SE) was significantly higher over Reef A than the mudflat (–512 ± 21 vs. –56.3 ± 10 mmol m^{-2} d^{-1}, n = 115 and 93, t = 23.6, p < 0.01) in June 2015. $Flux_{DARK}$ was slightly higher but not significantly different over Reef A than over Reef B in both August 2015 (–461 ± 33 vs. –428 ± 16 mmol m^{-2} d^{-1}, n = 53 and 129, t = 1.01, p = 0.32) and September 2015 (–167 ± 14 vs. –159 ± 10 mmol m^{-2} d^{-1}, n = 77 and 36, t = 0.41, p = 0.68). $Flux_{DARK}$ was significantly higher over Reef A than Reef C (–475 ± 19 vs. –300 ± 10 mmol m^{-2} d^{-1}, n = 97 and 101, t = 8.05, p < 0.01) in June and July 2016.

$Flux_{LIGHT}$ (± SE) was significantly higher over Reef A than the mudflat (–164 ± 20 vs. –29.4 ± 6.6 mmol m^{-2} d^{-1}, n = 74 and 66, t = 6.05, p < 0.01) in June 2015. $Flux_{LIGHT}$ was slightly lower but not significantly different over Reef A than over Reef B in August 2015 (–158 ± 22 vs. –178 ± 14 mmol m^{-2} d^{-1}, n = 39 and 63, t = 0.81, p = 0.42) and roughly equal in September 2015 (–117 ± 23 vs. –116 ± 20 mmol m^{-2} d^{-1}, n = 59 and 27, t = 0.04, p = 0.97). $Flux_{LIGHT}$ was slightly lower but not significantly different over Reef A than Reef C (–51.1 ± 14 vs. –61.1 ± 15 mmol m^{-2} d^{-1}, n = 62 and 75, t = 0.49, p = 0.63) in June and July 2016.

Tidal effects and controls of oxygen exchange

All 4 study sites were in the intertidal zone, and thus had different locations of the measurement footprint as determined by the direction of the flood and ebb tides. At all 3 oyster reefs, both flow speed and

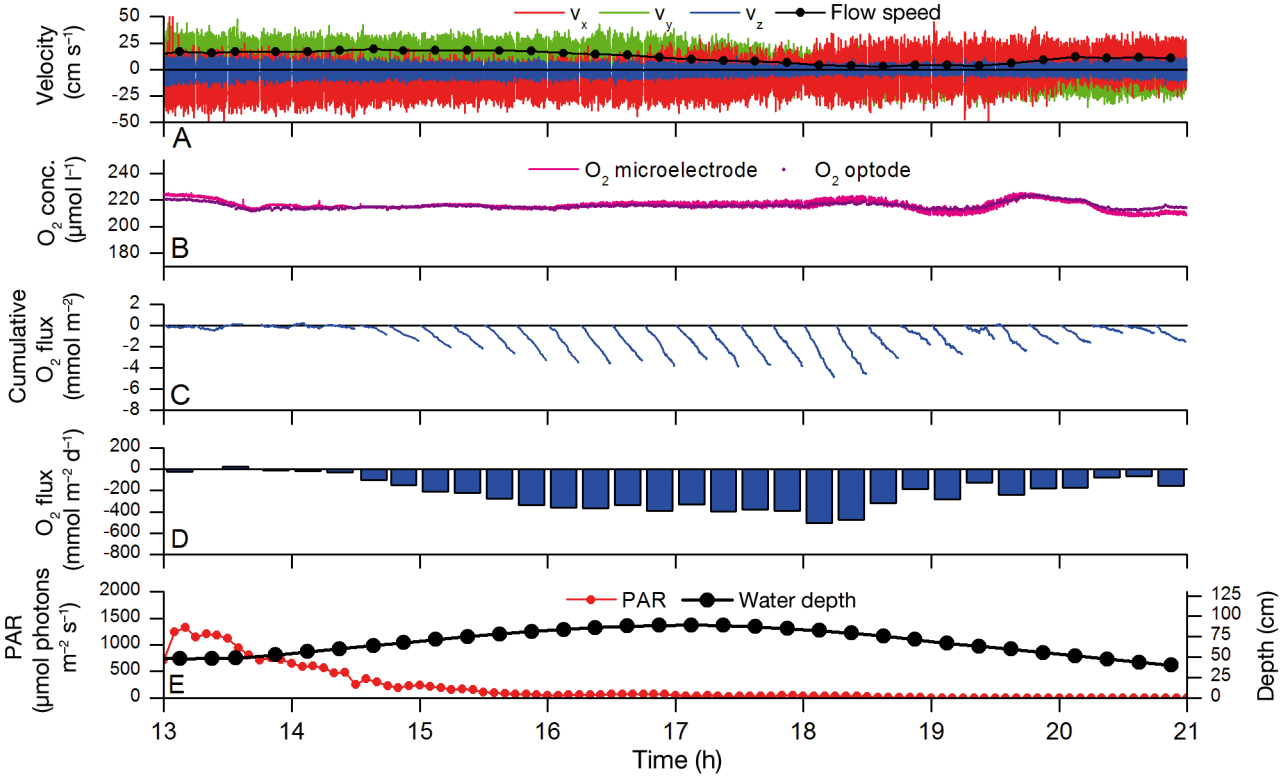

Fig. 5. Example eddy covariance data from Reef A showing (A) velocity, (B) oxygen concentration recorded by the Clark microelectrode and optode, (C) 15 min cumulative oxygen flux, (D) total oxygen flux, and (E) depth and photosynthetically active radiation (PAR). These data were taken during the afternoon and evening of 23 September 2015. Note that oxygen flux to the benthos is greater at lower PAR levels. This effect is attributed largely to microalgal primary production

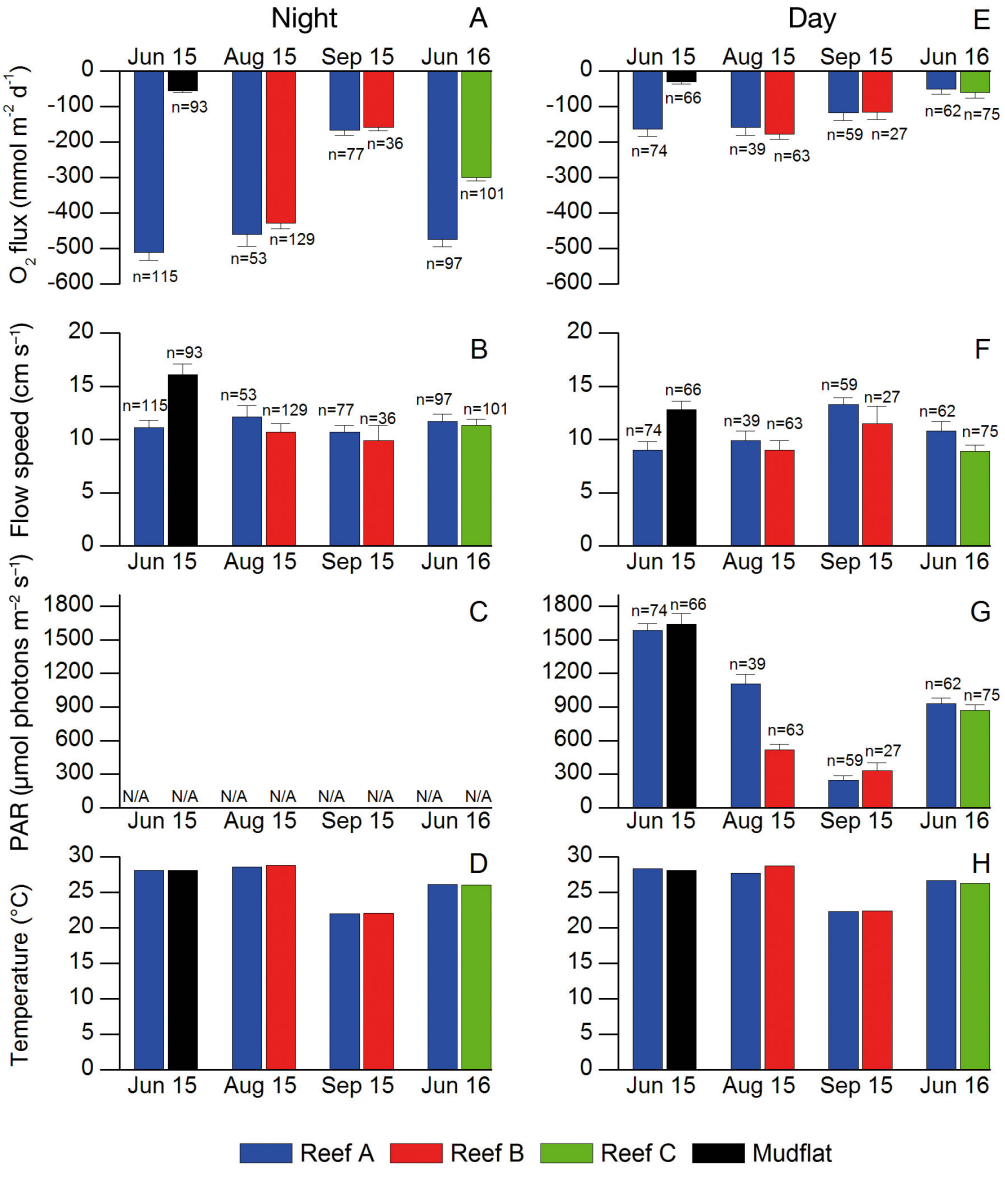

Fig. 6. Average (A,E) oxygen flux, (B, F) flow speed, (C,G) photosynthetically active radiation (PAR), and (D,H) temperature at each site for both nighttime and daytime deployments. Error bars represent standard errors, and n values are number of 15 min bursts used to calculate each average. Average nighttime (A) and daytime (E) oxygen flux are equivalent to $Flux_{DARK}$ and $Flux_{LIGHT}$, respectively

nighttime oxygen uptake were significantly higher for ebb conditions than flood conditions. Flow speed has been shown to be a major driver of nighttime oxygen uptake over oyster reefs (Reidenbach et al. 2013). In order to test the effect of tidal direction on nighttime oxygen uptake, we compared the average nighttime uptake between flood and ebb tides for data in which flow speed was below a certain threshold. This threshold needed to give similar mean values of flow speed for both flood and ebb tides while including as many data as possible. Balancing these 2 considerations, we chose a cutoff of 8 cm s^{-1} for the oyster reefs and 14 cm s^{-1} for the mudflat. Only summer data were used for this analysis to remove the potential impact of seasonality.

When accounting for flow speed, both Reef A and Reef C had significantly greater nighttime oxygen flux during ebb conditions than flood conditions (mean ± SE) (Reef A: −600 ± 43 vs. −410 ± 22 mmol m^{-2} d^{-1}, n = 38 and 71, $t = 4.35$, $p < 0.01$; Reef C: −341 ± 27 vs. −240 ± 24 mmol m^{-2} d^{-1}, n = 13 and 19, $t = 2.74$, $p = 0.01$). Reef B and the mudflat both had slightly greater but not significantly different nighttime oxygen flux during ebb conditions than flood conditions (Reef B: −380 ± 36

vs. –350 ± 27 mmol m^{-2} d^{-1}, n = 22 and 51, t = 0.64, p = 0.52; mudflat: –54.2 ± 11 vs. –44.7 ± 7.0 mmol m^{-2} d^{-1}, n = 21 and 27, t = 0.75, p = 0.46). These results, along with mean velocities and oxygen concentrations over the same data, are summarized in Fig. 7.

As there were no tidal direction effects at either Reef B or the mudflat, we were able to test the effect of flow speed on oxygen uptake at these 2 sites. At both Reef B and the mudflat, flow speed had a significant ($p < 0.05$) impact on oxygen flux (Fig. 8). For these analyses, only nighttime data were used to remove the impact of oxygen production due to photosynthesis by algae located on the reef. The few positive fluxes at low flow speed seen in Fig. 8 were attributed to measurement bias caused by horizontal advection of oxygen across the study sites (Holtappels et al. 2013). This bias occurs randomly in both directions, and evens out when averaging across all data. There was no effect of velocity on oxygen flux at either Reef A or Reef C once tidal direction was accounted for (Fig. 7). The reason for this lack of effect is unclear, and requires further investigation.

PAR had a significant effect on daytime oxygen flux over Reef A and Reef C in June and July 2016 ($p < 0.01$; Fig. 9). Although fluxes were rarely positive, they were less negative at higher PAR levels due to microalgal photosynthetic response to light. These 2 deployments were chosen as representative for PAR analysis because PAR levels were not consistent over Reef A and Reef B in August 2015, and were considerably lower in September 2015 (Fig. 6). Based on Fig. 9, Reef A had a light compensation point (x-intercept) of 2200 µmol photons m^{-2} s^{-1}, and Reef C had a light compensation point of 1250 µmol photons m^{-2} s^{-1}. The light compensation point for Reef A was above the maximum PAR viewed over this reef, whereas PAR levels were above the light compensation point at Reef C approximately 15% of the time.

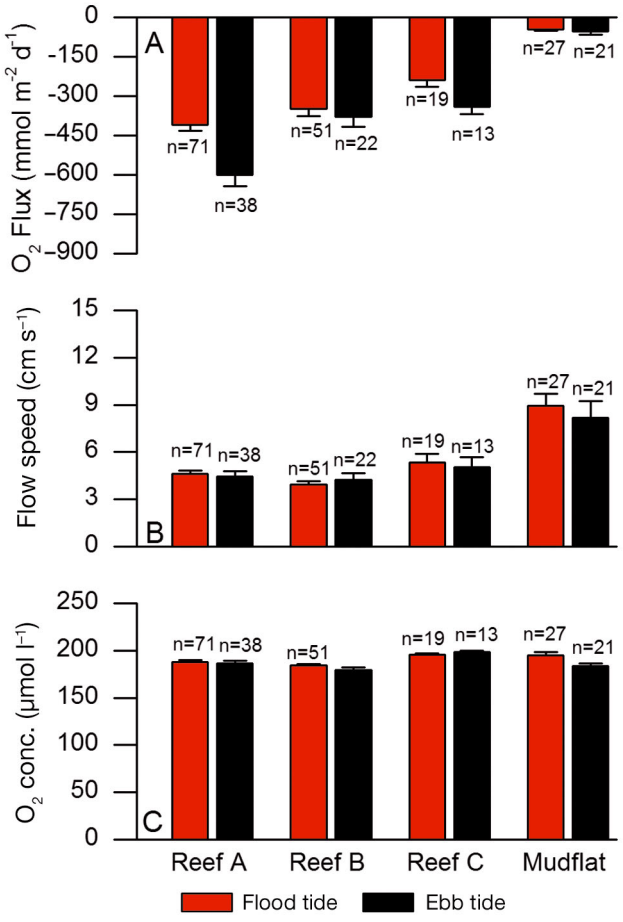

Fig. 7. Difference in mean (±SE) (A) oxygen flux, (B) flow speed, and (C) oxygen concentration between flood and ebb tide for all bursts where velocity was <8 cm s^{-1} for oyster reefs and <14 cm s^{-1} for mudflat. At all 4 sites, mean ebb flux was greater than mean flood flux when accounting for velocity differences, although this effect was only significant over Reef A and Reef C. Only summer nighttime bursts were used for this analysis

Day/night differences in flux and NEM

For all sites, $Flux_{DARK}$ was greater in magnitude than $Flux_{LIGHT}$ (Fig. 6). The difference between $Flux_{DARK}$ and $Flux_{LIGHT}$ for June 2015 was more than 12× greater over Reef A than over the mudflat (348 ± 29 vs. 27 ± 8 mmol m^{-2} d^{-1}; mean ± SE), and was consistently greater over Reef A than over Reef B or Reef C (Fig. 10).

NEM values showed all systems to be significantly heterotrophic, and were more than 7× greater for Reef A than the mudflat (–298 ± 15 vs. –40 ± 4 mmol m^{-2} d^{-1}; mean ± SE). NEM was roughly equal between Reef A and Reef B, and was greater for Reef A than Reef C (Fig. 10).

Hydrodynamics

The values for u_*, z_0, C_D, footprint length, and distance to maximum flux contribution are presented in Table 1. Values of C_D generally agreed with past measurements of drag over oyster reefs (Whitman & Reidenbach 2012, Styles 2015) and bare mud (Gross & Nowell 1983). At all 3 oyster sites, the size of the footprint indicates that the reefs contributed ≥80% of the measured oxygen flux (Table 1).

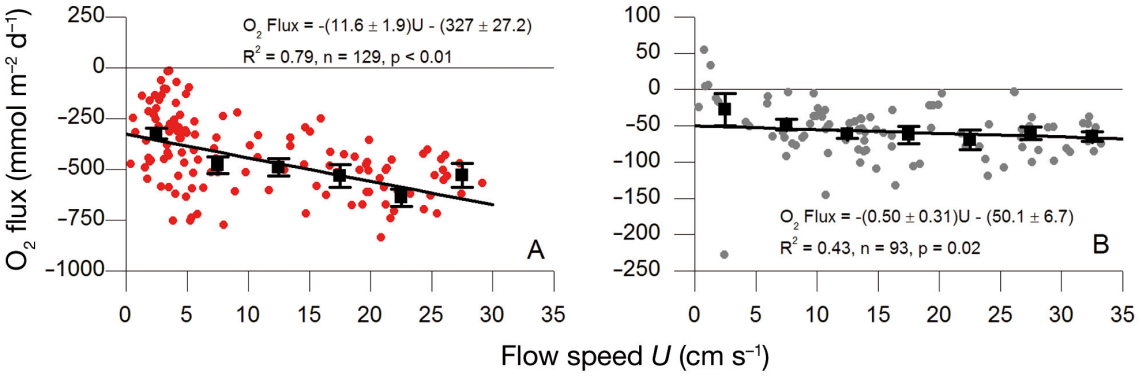

Fig. 8. Nighttime oxygen flux vs. flow speed over (A) Reef B and (B) mudflat. The data include both flood and ebb tides. Best fit and R^2 values describe binned data, n and p values describe unbinned data. There was no effect of velocity on oxygen flux at either Reef A or Reef C once tidal direction was accounted for. The reason for this lack of effect is unclear, and requires further investigation

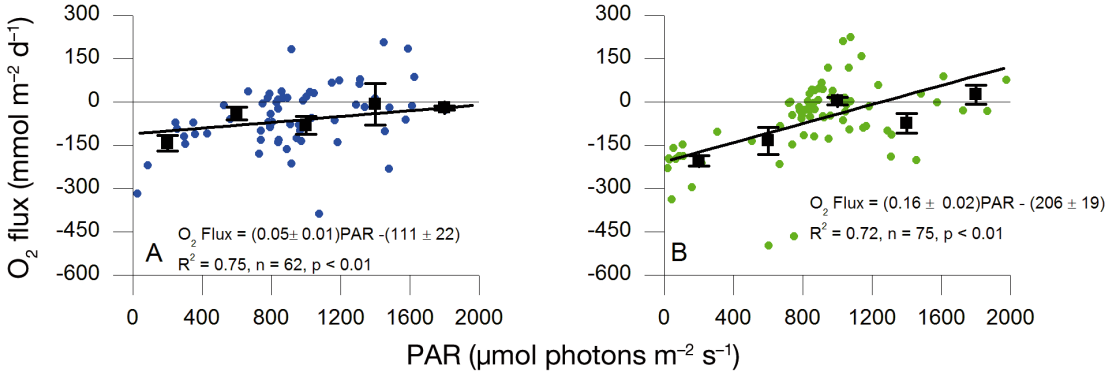

Fig. 9. Daytime oxygen flux vs. photosynthetically active radiation (PAR) at (A) Reef A and (B) Reef C. The decrease in uptake with increasing light levels is attributed to enhanced microalgal photosynthetic release of oxygen. These data were taken during the daytime in June and July 2016. These 2 deployments were chosen because PAR was not consistent over Reef A and Reef B in August 2015, and was much lower in September 2015. Each data point represents one 15 min burst. Best fit and R^2 values describe binned data, n and p values describe unbinned data

Normalized data

In order to better facilitate comparisons across all 4 sites, oyster density, $Flux_{DARK}$, and day/night flux differences were normalized against values for the natural Reef A. These results show similar trends across all 3 variables (Fig. 11) and also emphasize the high metabolic activity of the oyster reefs relative to the mudflat.

Finally, we examined oxygen demand per oyster. Reef A had a slightly smaller $Flux_{DARK}$ per oyster than Reef B and Reef C; however, values were similar at all 3 sites. Reef A had an oxygen demand (mean ± SE) of −1.75 ± 0.50 mmol m^{-2} d^{-1} per oyster, Reef B had a demand of −2.31 ± 0.34 mmol m^{-2} d^{-1} per oyster, and Reef C had a demand of −2.30 ± 1.05 mmol m^{-2} d^{-1} per oyster. It should be noted that the 0.25 m × 0.25 m quadrats used to determine reef oyster density were placed randomly on the different reefs. It is thus possible that the density closer to the eddy systems differs from the mean density of the reefs as a whole, which would affect these per oyster flux results.

DISCUSSION

Nighttime oxygen uptake

$Flux_{DARK}$ values over the oyster reefs ranged from a low of −300 mmol m^{-2} d^{-1} over Reef C in June and July 2016 to a high of −512 mmol m^{-2} d^{-1} over Reef A in June 2015 (Fig. 6). These results fall into the range of nighttime fluxes (−100 to −600 mmol m^{-2} d^{-1}) measured using aquatic eddy covariance over a nearby natural oyster reef by Reidenbach et al. (2013), but were lower than values measured using chamber incubations by Kellogg et al. (2013; −932 mmol m^{-2} d^{-1}),

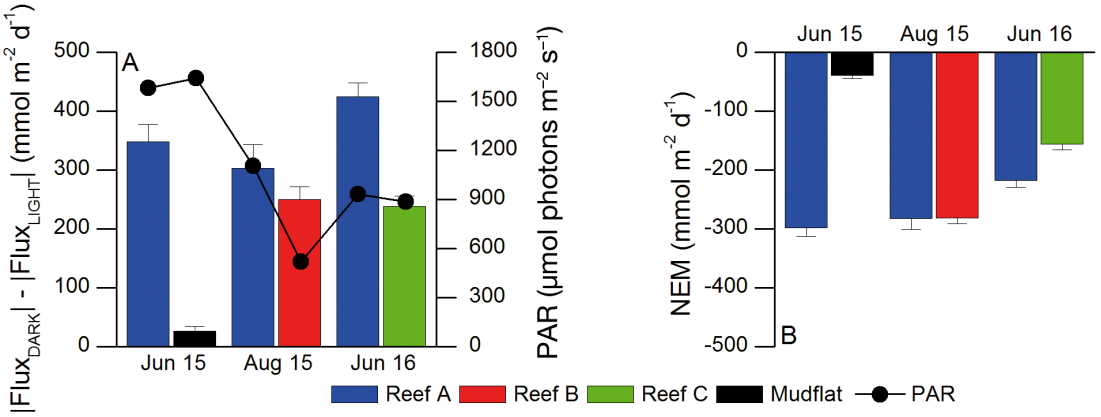

Fig. 10. (A) Summer differences between the absolute values of $Flux_{DARK}$ and $Flux_{LIGHT}$ and (B) net ecosystem metabolism (NEM) at all sites, with error bars representing accumulated standard error. Mean photosynthetically active radiation (PAR) values for each deployment are also shown for context. The difference between $Flux_{DARK}$ and $Flux_{LIGHT}$ is often used as an estimate of gross primary production, but this methodology may not be appropriate for this study (described in the 'Discussion'). NEM was calculated as the weighted average between $Flux_{LIGHT}$ and $Flux_{DARK}$ based on mean day length. NEM values show that oyster reefs are strongly heterotrophic systems, meaning they require external input of organic material. The source of this material is presumably phytoplankton filtered by the oysters

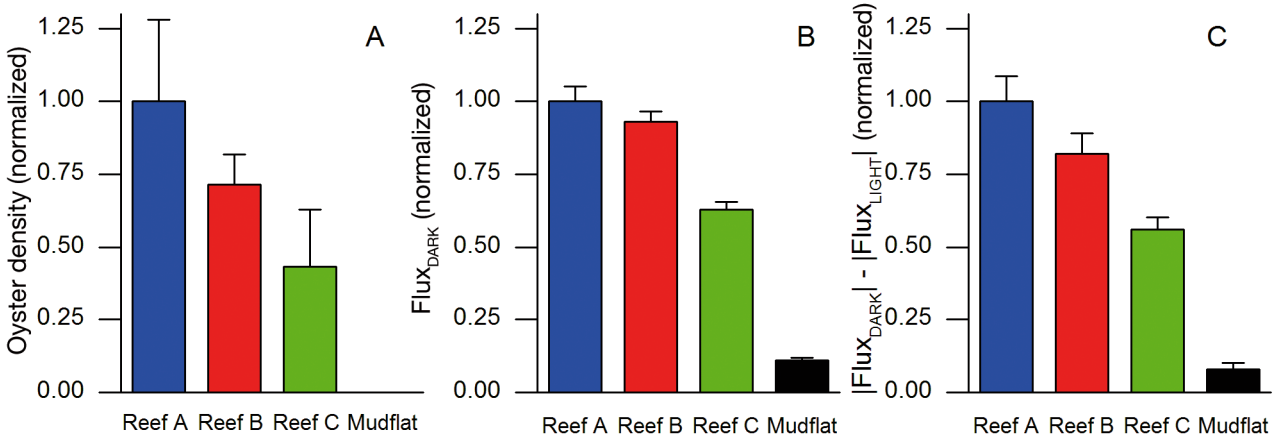

Fig. 11. (A) Oyster density, (B) $Flux_{DARK}$, and (C) $|Flux_{DARK}| - |Flux_{LIGHT}|$ normalized against Reef A. As oyster density decreases, both $Flux_{DARK}$ and differences between nighttime and daytime fluxes decrease as well. For all sites, the data were normalized by Reef A data taken from the same deployment, and only August 2015 data were used to normalize Reef B. Note that $Flux_{DARK}$ values are negative, indicating a net uptake of oxygen. Error bars represent accumulated standard errors

Table 1. Hydrodynamic and footprint characteristics of oyster reefs. The mature Reef A had the greatest benthic roughness, as shown by its relatively high values of the drag coefficient (C_D) and sediment surface roughness parameter (z_0). The size of the footprint is defined as the benthic surface area that contributes 90% of the measured flux. The size of the 80% contribution is approximately half this size (Berg et al. 2007), so over all reefs, more than 80% of the measured oxygen flux came from the reefs. Data from 18 June 2015 were used for the mudflat and Reef A, data from 27 September 2015 were used for Reef B, and data from 6 July 2016 were used for Reef C. All values represent means ± SE. Bursts with velocity <2 cm s^{-1} were removed from this analysis, as were any negative values for footprint length or distance to maximum flux contribution

Site	Density (oysters m^{-2}) (n)	Length (m)	Width (m)	n	u_* (cm s^{-1})	z_0 (cm)	C_D	Footprint length (m)	Max contribution (m)
Reef A	350 ± 62 (4)	22.5	10.5	38	1.78 ± 0.09	1.30 ± 0.19	0.054 ± 0.01	24 ± 3	0.35 ± 0.05
Reef B	295 ± 35 (4)	27.0	16.0	51	1.42 ± 0.08	0.64 ± 0.04	0.022 ± 0.00	18 ± 1	0.34 ± 0.02
Reef C	186 ± 66 (7)	77.5	44.5	45	1.44 ± 0.08	0.54 ± 0.10	0.023 ± 0.01	32 ± 2	0.47 ± 0.02
Mudflat	–	–	–	56	1.13 ± 0.06	0.07 ± 0.03	0.006 ± 0.001	56 ± 3	0.33 ± 0.13

Kellogg et al. (2014; –703 mmol m^{-2} d^{-1}), and Humphries et al. (2016; –677 mmol m^{-2} d^{-1}). Besides possible differences in oyster density, there are a few reasons why past incubation fluxes might have been greater than eddy covariance measurements. These incubations were not performed under true *in situ* conditions, either because they were conducted *ex situ* in a laboratory (Kellogg et al. 2013, 2014), or because the presence of chambers altered natural flow conditions (Humphries et al. 2016). *Ex situ* incubations involve removing a column of sediment from the natural environment, a process that can expose labile organic material that was previously buried (Hulthe et al. 1998) as well as release previously reduced inorganic compounds (Almroth et al. 2009). Both of these impacts may result in enhanced oxygen uptake relative to natural values.

Seasonal differences in $Flux_{DARK}$ values generally agreed with past incubation studies (Kellogg et al. 2013, Humphries et al. 2016). Reef A and Reef B were the only sites that were sampled in both the summer and the fall, and for both sites, $Flux_{DARK}$ fell by 63% from August 2015 to September 2015 (–461 to –167 mmol m^{-2} d^{-1} for Reef A, –428 to –158 mmol m^{-2} d^{-1} for Reef B; Fig. 6). This seasonal decline matches those given by Kellogg et al. (2013), who recorded a 67% decline from June to November, and Humphries et al. (2016), who reported a 66% decrease from summer to fall. These declines in oxygen uptake are possibly attributable to lower temperature suppressing oyster activity, as mean temperature for our study was ~6°C lower in September 2015 (22°C) than August 2015 (28°C; Fig. 6).

Oyster $Flux_{DARK}$ values were comparable to nighttime eddy covariance measurements recorded over a nearby *Zostera marina* seagrass meadow (Rheuban et al. 2014a). Maximum seasonal respiration (equivalent to $Flux_{DARK}$) of this meadow was –440 mmol m^{-2} d^{-1} (Rheuban et al. 2014a), within the range of values measured over the reefs (Fig. 6). Despite similar values of nighttime oxygen uptake, seagrass meadows have a fundamentally different community structure than oyster reefs, as they are founded on a significant phototrophic rather than heterotrophic biomass. These differences are reflected in NEM values. Seagrass meadows range from slight heterotrophy to net autotrophy in summer months (Rheuban et al. 2014a), whereas all of our sites were strongly heterotrophic (Fig. 10). While the organic material necessary for summer meadow metabolism is primarily fixed by the seagrasses, oyster reefs require significant sources of exogenous carbon. These imports most likely come from phytoplankton advected through the water column, which represent the oysters' primary food source.

Mudflat metabolism was comparable to past eddy covariance measurements of unvegetated muddy subtidal sediments located near this same seagrass meadow (Hume et al. 2011, Rheuban et al. 2014b). Hume et al. (2011) reported a mean respiration for these sediments of –53 mmol m^{-2} d^{-1}, similar to our mudflat $Flux_{DARK}$ value of –56 mmol m^{-2} d^{-1}. Likewise, mean NEM was –35 mmol m^{-2} d^{-1} (Hume et al. 2011), close to our mudflat value of –40 mmol m^{-2} d^{-1}.

Sediments on the reefs can also contribute to the flux signal, as they may contain decomposing organic material and a build-up of reduced products from anaerobic decay processes, both of which can enhance $Flux_{DARK}$ values. Although we could not separate out the effects of oxygen uptake due to sediments on the reefs vs. that due to respiration by reef infauna and algae, these sediments likely contribute to the oxygen flux at a rate similar to that measured at the mudflat. $Flux_{DARK}$ values at Reef A and the mudflat were –512 and –56 mmol m^{-2} d^{-1}, respectively, in June 2015 (Fig. 6). The difference between these 2 values (–456 mmol m^{-2} d^{-1}) can likely be attributed to reef biota, and shows that respiration of reef organisms is approximately 8× greater than that of the surrounding sediment.

Controls of oxygen exchange and tidal effects

One strength of aquatic eddy covariance is a high temporal resolution of flux measurements (Rheuban & Berg 2013), which allows for the real-time correlation of oxygen flux with *in situ* environmental variables. In this study, we averaged fluxes over 15 min intervals, enabling us to identify short-term environmental drivers of oxygen exchange. In most benthic systems, the 2 main drivers of oxygen flux over these short time scales are light and flow speed (e.g. Hume et al. 2011, Berg et al. 2013, Long et al. 2013), and both of these were also found to impact oyster reef oxygen flux in this study.

PAR had a significant effect on daytime oxygen flux over the oyster reefs, with diminished oxygen uptake occurring at higher light levels. This effect was particularly present over Reef A and Reef C in June and July 2016 (Fig. 9), and is attributed to the stimulation of microalgal photosynthesis by PAR. Enhanced photosynthetic oxygen release by the algae counteracts uptake by the reef community, resulting in a decreasing net uptake of oxygen with increasing light levels.

Flow speed had a clear, significant effect on flux at 2 of the 4 sites in this study (Fig. 8), a relationship that has been shown in the past for oyster reefs (Reidenbach et al. 2013). Flow speed can stimulate oxygen uptake in benthic systems by several mechanisms, including by replenishing oxygen to anoxic permeable sediments (Huettel & Gust 1992) and by decreasing the thickness of the diffusive boundary layer for cohesive substrates (Bryant et al. 2010). However, due to the reefs' muddy sediments and complex vertical structure, the impact of these effects is expected to be relatively minor. Of possibly greater importance in these systems is the impact of flow speed on sediment deposition and resuspension. Reidenbach et al. (2013) showed that sediment flux over a nearby oyster reef was highly dependent on flow speed, with deposition stimulated by flow at lower (0–10 cm s^{-1}) speeds and net resuspension occurring at higher (>25 cm s^{-1}) speeds. Both sediment deposition (Glud 2008) as well as sediment resuspension (Glud 2008, Almroth et al. 2009) have been shown to stimulate oxygen consumption in marine systems, so the complex sediment dynamics of oyster reefs may drive much of the velocity effects seen here.

Given the intertidal nature of the sites, tides affect much of the functioning of these systems, including both light and flow velocity. PAR can be rapidly attenuated with depth in coastal waters (Babin et al. 2003), so at greater depths associated with high tide there will be greater net oxygen uptake due to lower PAR reaching the benthos. Flow speeds at all sites were also much higher during ebb tide than flood tide, which may have contributed to higher uptake during ebb conditions vs. flood conditions. At 2 of the 4 sites sampled (Reef A and Reef C) there were significant differences in nighttime oxygen uptake between flood and ebb tides which were not attributable to possible flow speed effects (Fig. 7). This tidal effect may be partially attributed to heterogeneity on the reefs, with greater densities of oysters in the ebb tide footprint vs. the flood tide footprint of both reefs. It could also be due to enhanced sediment resuspension that occurs during ebb conditions when flow drains from the shallow mudflats to the deeper tidal channels (Reidenbach et al. 2013).

Diurnal patterns in oxygen flux

All sites in this study showed significant differences between $Flux_{DARK}$ and $Flux_{LIGHT}$, ranging from 27 mmol m^{-2} d^{-1} over the mudflat to 239–424 mmol m^{-2} d^{-1} over the oyster reefs (Fig. 10). Studies performed using *ex situ* sediment incubations often define these differences between dark and light flux as the gross primary production (GPP) (e.g. Welsh et al. 2000, Kellogg et al. 2014), and applying this approach to the mudflat results in a comparable GPP to the mean value previously reported over muddy subtidal sediments in a nearby lagoon (18 mmol m^{-2} d^{-1}; Hume et al. 2011). Applying this methodology to the oyster reefs, however, results in substantial GPP values that are comparable to summer values reported over a nearby densely vegetated seagrass meadow (~200–475 mmol m^{-2} d^{-1}; Rheuban et al. 2014a). While algal photosynthesis on the reefs likely accounts for much of the considerable differences between daytime and nighttime uptake, other factors including our sampling methodology and possible diurnal rhythms in oyster respiration (described below) may also inflate these day/night differences above the true reef GPP.

Algal photosynthesis is an important driver of day/night differences (Fig. 5), evidenced by significant decreases in uptake that occurred at higher light levels (Fig. 9). Dame et al. (1992) found large levels of primary production over oyster reefs during months when there were large quantities of benthic macroalgae, but daily to semi-daily visual inspections of the reefs sampled here showed minimal amounts of macroalgae with the exception of Reef C. Therefore, production at our sites is attributed primarily to high densities and/or photosynthetic rates of benthic microalgae on the oyster reefs. Benthic microalgal production can be substantial in shallow coastal environments (e.g. Varela & Penas 1985, Rysgaard et al. 1995, Eyre & Ferguson 2002), and there are several possible ways by which it may be further enhanced by the presence of oyster reefs. These systems are highly rugose and vertically complex, which greatly increases the total vs. planar surface area and allows the reefs to host greater quantities of benthic algae than flatter surfaces such as bare sediments. A similar increase in 3-dimensionality has been shown to enhance coral reef oxygen production, resulting in averaged GPP as high as ~950 mmol m^{-2} d^{-1} (Long et al. 2013). Additionally, nutrients and carbon dioxide released by oysters can possibly enhance rates of microalgal photosynthesis, as benthic microalgae have been shown to take up nitrogen compounds released by oysters (Kellogg et al. 2014). Both of these factors would explain why day/night differences in uptake scaled with oyster density (Fig. 11). Kellogg et al. (2014) found increases in primary production that scaled with oyster biomass, which they attributed to oyster nutrient efflux stimulating algal photo-

synthesis. In our study, Reef A had the highest oyster density and day/night differences (Fig. 11), as well as the largest values of z_0 and C_D (Table 1). These results agree with visual inspections of the reefs, and imply that Reef A had the greatest vertical complexity and thus the highest surface area for algae to grow.

The sampling protocol used in this study may also account for part of the large differences between $Flux_{DARK}$ and $Flux_{LIGHT}$. Summer daytime data collection intervals were centered around noon (described in the 'Materials and methods'), meaning $Flux_{LIGHT}$ values likely indicate near-minimum oxygen uptake, and differences between $Flux_{DARK}$ and $Flux_{LIGHT}$ may represent near-maximum production by the reef community. Our results are therefore perhaps more comparable to maximum oxygen production values reported in other systems. For example, Rheuban et al. (2014a) reported mid-day seagrass oxygen production exceeding 1000 mmol m^{-2} d^{-1}, values which are far greater than both their reported GPP and the day/night differences presented here. Additionally, for all of our sites, mean flow speed was higher during the night than during the day for summer measurements (Fig. 6). Flow speed can stimulate reef oxygen consumption through several mechanisms, including by impacting the reef sediment flux (described above), so part of these diurnal differences in flux may also be attributed to higher flow speeds stimulating greater nighttime vs. daytime oxygen uptake.

In order to use differences between $Flux_{DARK}$ and $Flux_{LIGHT}$ to estimate GPP, it is necessary to assume that the gross amount of oxygen consumed by the reefs (by both biological and chemical processes) is constant across the diurnal cycle, and that any difference in net oxygen uptake between day and night is attributed solely to daytime oxygen release by primary producers. This is a standard assumption for most flux studies conducted in phototrophic systems, such as seagrass meadows or algal beds (e.g. Hume et al. 2011, Rheuban et al. 2014a,b, Attard et al. 2015). However, previous research into the circadian rhythms of bivalve species has shown that feeding activity (and thus respiration) may in fact vary diurnally. *In situ* measurements of blue mussels *Mytilus edulis* have shown that they increase both the extent and frequency of valve opening at night vs. in the daytime, with the extent of valve opening being negatively correlated to light intensity (Wilson et al. 2005). These results imply that respiration for *M. edulis* beds may be greater at night than during the day. Similar behavior in oysters would partially explain the large differences measured between daytime and nighttime oxygen uptake. However, this pattern is not consistent across all bivalve species (e.g. Mat et al. 2014), and further research into the circadian rhythmicity of *Crassostrea virginica* is needed.

Implications for reef restoration

Our results suggest that $Flux_{DARK}$ scales closely with oyster population density (Fig. 11), with summer values ranging from −1.8 to −2.3 mmol m^{-2} d^{-1} $oyster^{-1}$. Similar values were found by Boucher & Boucher-Rodoni (1988), who measured the oxygen uptake of transplanted *C. gigas* oysters via *in situ* dark enclosure incubations and recorded a mean June flux of around −2.6 mmol m^{-2} d^{-1} $oyster^{-1}$. These results also agree with Kellogg et al. (2014), who found an increase in oxygen uptake with oyster biomass.

It is important to note that oyster densities in this study were determined using quadrats placed randomly on the different reefs. Although the eddy covariance flux integrates over a large benthic surface area (18–56 m in length; Table 1), the location of the greatest contribution to the measured flux is relatively close to the eddy system (Berg et al. 2007). For our reefs, this location was approximately 0.3 to 0.5 m upstream of the eddy system (Table 1). It is therefore possible that the density within the immediate vicinity of the eddy system differed from the average density of the reef as a whole, which would affect our per oyster flux estimates. Additionally, we did not conduct measurements of biomass and/or shell lengths of oysters, which are often reported in the literature (e.g. Dame et al. 1992, Kellogg et al. 2013, 2014). Quantifying oyster biomass and shell length values, as well as sampling oyster densities closer to the eddy systems, may have allowed us to better constrain our results and to more accurately compare them with past studies.

The vertical extent of oyster reefs is an important goal of reef restoration, as it helps prevent sedimentation of the reef (Schulte et al. 2009) as well as attract pelagic oyster larvae necessary for reef accretion (Fuchs & Reidenbach 2013, Fuchs et al. 2015). However, our results indicate it has little effect on ecosystem metabolism. Although Reef A had far greater values of z_0 and C_D than Reef B (Table 1), these 2 sites had similar values of NEM (Fig. 10) and $Flux_{DARK}$ (Fig. 11). Likewise, despite having approximately equal z_0 and C_D (Table 1), Reef B had much

higher NEM (Fig. 10) and $Flux_{DARK}$ (Fig. 11) values than Reef C. Thus the restoration of oxygen metabolism and ecosystem functioning as reefs mature is spurred primarily by an increase in oyster density, and not by the vertical structure of the reef itself.

Oxygen uptake by oyster reefs is positively correlated with denitrification (Kellogg et al. 2013, Humphries et al. 2016, Smyth et al. 2016). Humphries et al. (2016) even suggested that resource managers may want to measure oxygen flux as a proxy for the removal of nitrogen from the water column, although this requires further investigation. Due to the fact that $Flux_{DARK}$ scaled with oyster density (despite possible uncertainties in our density measurements), it is also a possible measure of restoration success. By using Reef A, a fully developed natural reef, as a baseline and the mudflat as a control, we can quantify the relative success of restoring benthic exchange to restoration Reefs B and C. If we assume that these reefs are in a relatively healthy condition (i.e. minimal dead and decomposing oysters, which were not observed on the reefs), then Reef B, which was constructed in 2010, appears to be nearly as functional as the natural Reef A. Reef C, established in 2008, has been less successful, as it showed only ~60% of the oxygen demand and ~50% of the oyster density of Reef A (Fig. 11). Our results suggest that true *in situ* measurements of oxygen fluxes can give key insight into the functioning, health, and state of restoration of oyster reef communities. When possible, such measurements can be a beneficial part of oyster reef monitoring programs.

Acknowledgements. We thank B. Lusk and The Nature Conservancy for providing access to the sites as well as background information on the oyster reefs. We also thank D. Boyd and T. Byrd for field assistance, and acknowledge the efforts of the late A. Schwarzschild in providing research support. Support for this study was provided by the National Science Foundation (NSF) through grants for the Virginia Coast Reserve Long-Term Ecological Research program (DEB-0621014 and DEB-1237733), Chemical Oceanography program (OCE-1334848) to P.B., and a CAREER Grant to M.A.R. (OCE-1151314). Support was also provided by the University of Virginia.

LITERATURE CITED

Almroth E, Tengberg A, Andersson JH, Pakhomova S, Hall POJ (2009) Effects of resuspension on benthic fluxes of oxygen, nutrients, dissolved inorganic carbon, iron and manganese in the Gulf of Finland, Baltic Sea. Cont Shelf Res 29:807–818

Attard KM, Stahl H, Kamenos NA, Turner G, Burdett HL, Glud RN (2015) Benthic oxygen exchange in a live coralline algal bed and an adjacent sandy habitat: an eddy covariance study. Mar Ecol Prog Ser 535:99–115

Babin M, Morel A, Fournier-Sicre V, Fell F, Stramski D (2003) Light scattering properties of marine particles in coastal and open ocean waters as related to the particle mass concentration. Limnol Oceanogr 48:843–859

Beck MW, Brumbaugh RD, Airoldi L, Carranza A and others (2011) Oyster reefs at risk and recommendations for conservation, restoration, and management. Bioscience 61: 107–116

Berg P, Huettel M (2008) Monitoring the seafloor using the noninvasive eddy correlation technique: integrated benthic exchange dynamics. Oceanography 21:164–167

Berg P, Røy H, Janssen F, Meyer V, Jørgensen BB, Huettel M, de Beer D (2003) Oxygen uptake by aquatic sediments measured with a novel non-invasive eddy correlation technique. Mar Ecol Prog Ser 261:75–83

Berg P, Røy H, Wiberg P (2007) Eddy correlation flux measurements: the sediment surface area that contributes to the flux. Limnol Oceanogr 52:1672–1684

Berg P, Glud RN, Hume A, Stahl H, Oguri K, Meyer V, Kitazato H (2009) Eddy correlation measurements of oxygen uptake in deep ocean sediments. Limnol Oceanogr Methods 7:576–584

Berg P, Long MH, Huettel M, Rheuban JE and others (2013) Eddy correlation measurements of oxygen fluxes in permeable sediments exposed to varying current flows and light. Limnol Oceanogr 58:1329–1343

Berg P, Reimers CE, Rosman JH, Huettel M, Delgard ML, Reidenbach MA, Özkan-Haller HT (2015) Technical note: time lag correction of aquatic eddy covariance data measured in the presence of waves. Biogeosciences 12: 6721–6735

Boucher G, Boucher-Rodoni R (1988) In situ measurement of respiratory metabolism and nitrogen fluxes at the interface of oyster beds. Mar Ecol Prog Ser 44:229–238

Bryant LD, Lorrai C, McGinnis DF, Brand A, Wüest A, Little JC (2010) Variable sediment oxygen uptake in response to dynamic forcing. Limnol Oceanogr 55:950–964.

Coen LD, Brumbaugh RD, Bushkek D, Grizzle R and others (2007) Ecosystem services related to oyster restoration. Mar Ecol Prog Ser 341:303–307

Dade WB, Hogg AJ, Boudreau BP (2001) Physics of flow above the sediment-water interface. In: Boudreau BP, Jørgensen BB (eds) The benthic boundary layer. Oxford University Press, New York, NY, p 3–43

Dame RF, Spurrier JD, Zingmark RG (1992) In situ metabolism of an oyster reef. J Exp Mar Biol Ecol 164:147–159

Eyre BD, Ferguson AJP (2002) Comparison of carbon production and decomposition, benthic nutrient fluxes and denitrification in seagrass, phytoplankton, benthic microalgae- and macroalgae- dominated warm-temperate Australian lagoons. Mar Ecol Prog Ser 229:43–59

Fuchs HL, Reidenbach MA (2013) Biophysical constraints and optimal patch lengths for settlement of a reef-building bivalve. PLOS ONE 8:e71506

Fuchs HL, Gerbi GP, Hunter EJ, Christman AJ, Diez FJ (2015) Hydrodynamic sensing and behavior by oyster larvae in turbulence and waves. J Exp Biol 218: 1419–1432

Glud RN (2008) Oxygen dynamics of marine sediments. Mar Biol Res 4:243–289

Glud RN, Berg P, Hume A, Batty P, Blicher ME, Lennert K, Rysgaard S (2010) Benthic O_2 exchange across hard-bottom substrates quantified by eddy correlation in a sub-Arctic fjord. Mar Ecol Prog Ser 417:1–12

Gross TF, Nowell AR (1983) Mean flow and turbulence scal-

ing in a tidal boundary layer. Cont Shelf Res 2:109–126
Holtappels, M, Glud RN, Donis D, Liu B, Hume A, Wenzhöfer F, Kuypers MMM (2013) Effects of transient bottom water currents and oxygen concentrations on benthic exchange rates as assessed by eddy correlation measurements. J Geophys Res Oceans 118:1157–1169
Holtappels M, Noss C, Hancke K, Cathalot C, McGinnis DF, Lorke A, Glud RN (2015) Aquatic eddy correlation: quantifying the artificial flux caused by stirring-sensitive O_2 sensors. PLOS ONE 10:e0116564
Hubbard AB, Reidenbach MA (2015) Effects of larval swimming behavior on the dispersal and settlement of the eastern oyster *Crassostrea virginica.* Mar Ecol Prog Ser 535:161–176
Huettel M, Gust G (1992) Solute release mechanisms from confined sediment cores in stirred benthic chambers and flume flows. Mar Ecol Prog Ser 82:187–197
Hulthe G, Hulth S, Hall POJ (1998) Effect of oxygen on degradation rate of refractory and labile organic matter in continental margin sediments. Geochim Cosmochim Acta 62:1319–1328
Hume A, Berg P, McGlathery KJ (2011) Dissolved oxygen fluxes and ecosystem metabolism in an eelgrass (*Zostera marina*) meadow measured with the eddy correlation technique. Limnol Oceanogr 56:86–96
Humphries AT, Ayvazian SG, Carey JC, Hancock BT and others (2016) Directly measured denitrification reveals oyster aquaculture and restored oyster reefs remove nitrogen at comparable high rates. Front Mar Sci 3:74
Jackson JBC, Kirby MX, Berger WH, Bjorndal KA and others (2001) Historical overfishing and the recent collapse of coastal ecosystems. Science 293:629–637
Kellogg ML, Cornwell JC, Owens MS, Paynter KT (2013) Denitrification and nutrient assimilation on a restored oyster reef. Mar Ecol Prog Ser 480:1–19
Kellogg ML, Cornwell JC, Owens MS, Luckenbach MW, Ross PG, Leggett TA (2014) Scaling ecosystem services to reef development: effects of oyster density on nitrogen removal and reef community structure. Virginia Institute of Marine Science, College of William & Mary, Gloucester Point, VA
Kemp WM, Boynton WR, Adolf JE, Boesch DF and others (2005) Eutrophication of Chesapeake Bay: historical trends and ecological interactions. Mar Ecol Prog Ser 303:1–29
Kirby MX (2004) Fishing down the coast: historical expansion and collapse of oyster fisheries along continental margins. Proc Natl Acad Sci USA 101:13096–13099
Lee X, Massman W, Law B (2004) Handbook of micrometeorology: a guide for surface flux measurement and analysis. Kluwer Academic Publishers, Dordrecht
Long MH, Rheuban JE, Berg P, Zieman JC (2012) A comparison and correction of light intensity loggers to photosynthetically active radiation sensors. Limnol Oceanogr Methods 10:416–424
Long MH, Berg P, de Beer D, Zieman JC (2013) In situ coral reef oxygen metabolism: an eddy correlation study. PLOS ONE 8:e58581
Long MH, Berg P, McGlathery KJ, Zieman JC (2015) Subtropical seagrass ecosystem metabolism measured by eddy covariance. Mar Ecol Prog Ser 529:75–90
Lorrai L, McGinnis DF, Berg P, Brand A, Wüest A (2010) Application of oxygen eddy correlation in aquatic systems. J Am Meteorol Soc 27:1533–1545
Lotze HK, Lenihan HS, Bourque BJ, Bradbury RH and others (2006) Depletion, degradation, and recovery potential of estuaries and coastal seas. Science 312:1806–1809
Mat AM, Massabuau JC, Ciret P, Tran D (2014) Looking for the clock mechanism responsible for circatidal behavior in the oyster *Crassostrea gigas.* Mar Biol 161:89–99
Nelson KA, Leonard LA, Posey MH, Alphin TD, Mallin MA (2004) Using transplanted oyster (*Crassostrea virginica*) beds to improve water quality in small tidal creeks: a pilot study. J Exp Mar Biol Ecol 298:347–368
Newell RIE (1988) Ecological changes in Chesapeake Bay: Are they the result of over harvesting the American oyster, *Crassostrea virginica*? In: Lynch MP, Krome EC (eds) Understanding the estuary: advances in Chesapeake Bay research. Chesapeake Research Consortium Publications 129. CBP/TRS 24/88. Chesapeake Research Consortium, Solomons, MD, p 536–546
Oliver LM, Fisher WS, Ford SE, Ragone Calvo LM, Burreson EM, Sutton EB, Gandy J (1998) *Perkinsus marinus* tissue distribution and seasonal variation in oysters *Crassostrea virginica* from Florida, Virginia and New York. Dis Aquat Org 34:51–61
Priestley C, Swinbank W (1947) Vertical transport of heat by turbulence in the atmosphere. Proc R Soc A 189:543–561
Reidenbach MA, Berg P, Hume A, Hansen JCR, Whitman ER (2013) Hydrodynamics of intertidal oyster reefs: the influence of boundary layer flow processes on sediment and oxygen exchange. Limnol Oceanogr Fluids Environ 3:225–239
Reimers CE, Özkan-Haller HT, Albright AT (2016) Microelectrode velocity effects and aquatic eddy covariance measurements under waves. J Atmos Ocean Technol 33: 263–282
Rheuban JE, Berg P (2013) The effects of spatial and temporal variability at the sediment surface on aquatic eddy correlation flux measurements. Limnol Oceanogr Methods 11:351–359
Rheuban JE, Berg P, McGlathery KJ (2014a) Multiple timescale processes drive ecosystem metabolism in eelgrass (*Zostera marina*) meadows. Mar Ecol Prog Ser 507:1–13
Rheuban JE, Berg P, McGlathery KJ (2014b) Ecosystem metabolism along a colonization gradient of eelgrass (*Zostera marina*) measured by eddy correlation. Limnol Oceanogr 59:1376–1387
Rodney WS, Paynter KT (2006) Comparisons of macrofaunal assemblages on restored and non-restored oyster reefs in mesohaline regions of Chesapeake Bay in Maryland. J Exp Mar Biol Ecol 335:39–51
Rothschild BJ, Ault JS, Goulletquer P, Héral M (1994) Decline of the Chesapeake Bay oyster population: a century of habitat destruction and overfishing. Mar Ecol Prog Ser 111:29–39
Rovelli L, Attard KM, Bryant LD, Flögel S and others (2015) Benthic O_2 uptake of two cold-water coral communities estimated with the non-invasive eddy correlation technique. Mar Ecol Prog Ser 525:97–104
Rysgaard S, Christensen PB, Nielsen LP (1995) Seasonal variation in nitrification and denitrification in estuarine sediment colonized by benthic microalgae and bioturbating infauna. Mar Ecol Prog Ser 126:111–121
Schlichting H, Gersten K (2000) Boundary layer theory, 8th edn. Springer, New York, NY
Schulte DM, Burke RP, Lipcius RN (2009) Unprecedented restoration of a native oyster metapopulation. Science 325:1124–1128
Smyth AR, Geraldi NR, Thompson SP, Piehler MF (2016)

Biological activity exceeds biogenic structure in influencing sediment nitrogen cycling in experimental oyster reefs. Mar Ecol Prog Ser 560:173–183

Styles R (2015) Flow and turbulence over an oyster reef. J Coast Res 31:978–985

Thomsen MS, McGlathery K (2006) Effects of accumulations of sediments and drift algae on recruitment of sessile organisms associated with oyster reefs. J Exp Mar Biol Ecol 328:22–34

Varela M, Penas E (1985) Primary production of benthic microalgae in an intertidal sand flat of the Ria de Arosa, NW Spain. Mar Ecol Prog Ser 25:111–119

Welsh DT, Bartoli M, Nizzoli D, Castaldelli G, Riou SA, Viaroli P (2000) Denitrification, nitrogen fixation, community primary productivity and inorganic-N and oxygen fluxes in an intertidal *Zostera noltii* meadow. Mar Ecol Prog Ser 208:65–77

Whitman ER, Reidenbach MA (2012) Benthic flow environments affect recruitment of *Crassostrea virginica* larvae to an intertidal oyster reef. Mar Ecol Prog Ser 463:177–191

Wiberg PL, Sherwood CR (2008) Calculating wave-generated bottom orbital velocities from surface-wave parameters. Comput Geosci 34:1243–1262

Wilson R, Reuter P, Wahl M (2005) Muscling in on mussels: new insights into bivalve behavior using vertebrate remote-sensing technology. Mar Biol 147:1165–1172

Editorial responsibility: Jana Davis, Annapolis, Maryland, USA

Submitted: April 28, 2017; Accepted: May 3, 2018
Proofs received from author(s): July 8, 2018